

AD A036032

2410

12

R-2016-PR  
October 1976

# Atmospheric Visual and Infrared Transmission Deduced from Surface Weather Observations: Weather and Warplanes VI

R. E. Huschke

D D C  
RECEIVED  
FEB 16 1977  
AUGUST 1976

A report prepared for  
UNITED STATES AIR FORCE PROJECT RAND

DIET  
Apr

**Rand**  
SANTA MONICA, CA. 90406

*Document should remain for public release as Mrs. Jelden Johnson,  
HQ USAF (RDQLR)*

*JEC  
2/25/77*

The research described in this report was sponsored by the United States Air Force under Contract No. F44620-73-C-0011 — Monitored by the Directorate of Planning, Programming and Analysis, Deputy Chief of Staff, Research and Development, Hq USAF.

Reports of The Rand Corporation do not necessarily reflect the opinions or policies of the sponsors of Rand research.

✓

A

R-2016-PR  
October 1976

# Atmospheric Visual and Infrared Transmission Deduced from Surface Weather Observations: Weather and Warplanes VI

R. E. Huschke

A report prepared for  
UNITED STATES AIR FORCE PROJECT RAND



PREFACE

The U.S. Air Force Project RAND research program at The Rand Corporation has for many years included studies of both target acquisition problems and weather effects on military operations. The work described in this report was supported by Project RAND under the study project "Science and Technology Research." It is a continuation of the weather-effects studies with application to target-acquisition modeling.

In the mainstream of target-acquisition modeling--at Rand and elsewhere--weather factors have traditionally entered in very simple terms that are difficult to relate to real, dynamic weather situations replete with significant time and space variability. To help correct this difficulty, the author has developed a method by which the quality of the atmospheric transmission of visible and infrared radiation (and imagery) can be quantitatively estimated directly from the hour-by-hour weather observations that are electronically archived for thousands of locations worldwide. Coupled with a target acquisition model, sensor characteristics, and tactical scenario, the method permits the direct evaluation of weapon system performance in any weather situation or climatic regime that can be extracted as a subset of the weather data base. One such evaluation recently completed at Rand using this modeling approach is reported in a forthcoming Rand report on the utility of an adverse-weather precision-guided munition in a NATO context.

As indicated by its subtitle ("Weather and Warplanes VI"), this report is preceded by five others that deal with the effects of weather and weather information on military systems and operations:

R-740-PR, *Use of Weather Information in Determining Cost/Performance and Force-Mix Tradeoffs: Weather and Warplanes I*, R. E. Huschke, June 1971 (Unclassified).

R-742-PR, *Ten Guidelines for the Simulation of Weather Sensitive Military Operations: Weather and Warplanes II*, R. E. Huschke, June 1971 (Unclassified).

R-774-PR, *A Simple Model to Elucidate the Utility of Weather Forecasting in Military Operations: Weather and Warplanes III*, R. R. Rapp, August 1971 (Unclassified).

R-1195-1-PR, *Tactical Airpower in NATO Contingencies--Modeling Weather Constraints on Air Operations: Weather and Warplanes IV* (U), R. E. Huschke, August 1973 (Confidential).

R-1349-PR, *Main Conclusions from the 'Weather-85' Study: Weather and Warplanes V* (U), R. E. Huschke, January 1974 (Secret).

This work should be of interest to Air Force and other DoD agencies concerned with assessing the effects of weather conditions on visual and 8-12  $\mu$ m infrared sensor systems.

## SUMMARY

New and remarkably effective weapons use visible and infrared imaging sensors to locate targets and automatically guide the missiles to their targets with great precision. The trouble is that weather conditions can, and in some parts of the world often do, deny these systems their needed capability to see through the atmosphere. A problem that arises, then, is how to predict the performance of different sensor systems in the weather conditions that characterize different places and times--that is, in the climates of a variety of potential theaters of battle.

World weather and climate are depicted in most relevant temporal and spatial detail by huge archives of surface weather observations from which subsets can be taken to represent almost any desired region, season, or time of day. From the information contained in surface weather observations, it is possible to infer visible and 8-12  $\mu\text{m}$  image transmission parameters, thereby opening the door to predicting sensor performance at (almost) any place of interest, including seasonal and diurnal effects.

Such common observables as cloud amount and height, visibility, precipitation, wind speed, temperature, dewpoint, and relative humidity permit construction of algorithms to make quantitative estimates of the following:

- o Visible extinction coefficient.
- o Sky-ground ratio.
- o 8-12  $\mu\text{m}$  extinction coefficient (including the aerosol extinction coefficient as well as the water vapor absorption coefficients).
- o Atmospheric vertical profiles of the relevant variables.

Some of these algorithms, notably the ones for sky-ground ratio and 8-12  $\mu\text{m}$  aerosol extinction, warrant strengthening by more field measurement studies and a broader application of theory than has been

supported to date. Another area that is seriously weak and has been addressed in only a tentative way is the effect of weather on the intrinsic nature of the target scene, especially the thermal (infrared) scene characteristics.

The Bailey and Mundie equations for the probability of target detection (Appendix A) supply a framework (one of several possible) for using the algorithms. The combination is a model called "WETTA" (weather effects on tactical target acquisition).

ACKNOWLEDGMENTS

The author wishes to thank Rand colleagues R. R. Rapp, Charles T. Kelley, Jr. and Jeannine Lamar for direct help in bringing this work to its present stage: Rapp for his continuous advocacy and technical help; Kelley for his leadership of the recent "Weather and PGMs" project, in which this work was first applied; and Lamar for her skillful computer programming. Other members of the Rand technical staff who provided support are H. H. Bailey, E. S. Batten, D. Deirmendjian, L. R. Koenig, L. G. Mundie and C. Schutz. The author also wishes to express appreciation for thorough technical reviews to H. H. Bailey and R. R. Rapp of Rand, and Lt. Col. R. F. Wachtmann, USAF, Director of Atmospheric and Space Sciences, Headquarters, Air Weather Service (MAC).



CONTENTS

PREFACE .....	iii
SUMMARY .....	v
ACKNOWLEDGMENTS .....	vii
Section	
I. INTRODUCTION .....	1
II. SURFACE WEATHER OBSERVATIONS .....	3
III. WETTA MODEL ALGORITHMS .....	6
Visible Extinction Coefficient .....	7
Sky-Ground Ratio .....	8
8-12 $\mu$ m Extinction Coefficient .....	13
Cloud-Free Line of Sight .....	18
Atmospheric Vertical Structure .....	19
IV. NEEDS FOR IMPROVEMENT .....	24
V. CONCLUDING REMARKS .....	28
Appendix	
A. TARGET DETECTION MODELING EQUATIONS (AFTER BAILEY AND MUNDIE) .....	29
REFERENCES .....	35

## I. INTRODUCTION

A trend in the U.S. and NATO military forces is to rely on effective weapons to help counteract the numerical superiority in armor and manpower held by Warsaw Pact forces. A major class of these new, effective weapons is the precision guided munitions (PGMs) that use optical sensing devices--the eye, television, or imaging infrared (IIR)--for target acquisition, lock-on, and terminal guidance. Such weapons vary in performance because weather varies in its degree of interference with the signals as they propagate from target to sensor. If a target can be effectively "seen" through the acquire/lock-on/launch/guide sequence, expected performance is excellent; otherwise, performance is nil.

Modern tactical warfare is apt to be more weather-sensitive than in the past, even as recently as in Vietnam. Weather has become a factor to be reckoned with seriously at all levels of weaponry decision-making. Procurement and deployment decisions require statistically valid predictions of PGM utility as a function of weather conditions in different potential theaters of combat at different times of year. Day-to-day and hour-to-hour decisions require adaptation of immediate weather forecasts to weapon loadout and target selection decisions.

The time and space variability of weather is well documented in a voluminous data base containing many years' history of hour-by-hour surface weather observations taken at thousands of locations worldwide. Each observation depicts the local state of the atmosphere but does not explicitly include several quantities that are needed to judge atmospheric effects on visual and infrared target-acquisition and missile-guidance systems. If these missing quantities could be inferred from the data that are contained in the observations, then the surface weather data base could become a valuable resource in making statistically valid predictions of weapon performance (including diurnal, seasonal, and geographic variability).

The model of weather effects on tactical target acquisition (WETTA)

described in this report is a collection of algorithms by which it is possible to estimate quantities used in mathematical formulations of visible and infrared radiation and image (contrast) transmission through the atmosphere from surface weather data. Some of the algorithms must be regarded as first approximations because they are attempts to quantify complex phenomena about which neither empirical nor theoretical understanding is yet sufficient to support firmly confident quantification.

Appendix A details the portions of the Bailey-Mundie [1,2] visual and infrared target acquisition models that have been adapted for use with the WETTA algorithms and applied to several practical problems, including a comparison of the utilities of TV (E-0) and imaging infrared (IIR) Maverick missiles in the context of an air-ground battle simulation used on a NATO central front scenario [3].

## II. SURFACE WEATHER OBSERVATIONS

The major weather services in the United States collect, use, and electronically file surface weather observations (as well as other types of observational data) originating throughout the world. For most defense-related applications, the primary source of these data is the United States Air Force Environmental Technical Applications Center (USAFETAC), Scott Air Force Base, Illinois, operated by the USAF Air Weather Service.

Over a period of about seven years, The Rand Corporation has accumulated a subset of the surface weather data base from USAFETAC for specific application in Rand studies. The Rand Weather Data Bank (RAWDAB) files now contain surface weather data on 93 locations in 22 countries; the observation intervals are mostly one hour and three hours, and the average period of record is about 12 years [4]. Table 1 lists,

Table 1

### RAWDAB FILES FOR GERMANY

Location	Dates of Record (mo/yr)		Observation Interval (hr)	Number of Observations
	From	To		
Berlin	3/46	12/63	1	155,468
Bitburg	3/52	12/67	1	135,521
Bremerhaven	1/49	11/71	3	45,424
Dresden	1/52	12/63	3	14,298
Emden-Hafen	4/60	11/71	3 <sup>a</sup>	12,902
Erfurt	1/59	12/63	3	12,535
Essen	1/49	11/71	3	62,268
Fulda	9/60	12/70	1 <sup>a</sup>	58,854
Grafenwöhr	6/62	12/70	1	75,247
Hamburg	1/49	11/71	1, 3	120,204
Hannover	1/49	11/71	1, 3	94,094
Heidelberg	4/51	12/70	1	172,595
Kitzingen	7/63	12/70	1	62,252
Leinefelde	1/52	12/60	6	13,025
Leipzig	1/52	12/60	6	12,907
Magdeburg	1/52	12/63	3, 6	22,796
Münster	8/59	11/71	3	32,594
Neubiberg	2/46	1/58	1	104,778

<sup>a</sup> Mainly daytime observations.

for illustration, the RAWDAB files for West and East Germany, including the dates of record, observation interval, and total number of observations for each location. The fact that locations having the same dates of record and observation interval have different numbers of observations (e.g., Hamburg and Hannover) serves as a warning that these data sets commonly contain both sporadic and systematic gaps that the user should be aware of.

Table 2 lists the meteorological information that is normally found in a surface weather observation. Those marked with "a" are the variables on which the visible and IR transmission algorithms are based. Ceiling height may or may not be included and cloud layer data may be more or less detailed, both depending on the type of weather code format used in the original compilation and transmission of the observation. In the present work, it is assumed that ceiling height is either given or is deduced from available cloud data.

Table 2  
INFORMATION NORMALLY CONTAINED IN A SURFACE  
WEATHER OBSERVATION

---

Atmospheric State Variables
Atmospheric pressure at station elevation
Atmospheric pressure reduced to sea level
Character and amount of 3-hour pressure change
Temperature (dry bulb) <sup>a</sup>
Temperature (wet bulb)
Dewpoint temperature <sup>a</sup>
Relative humidity <sup>a</sup>
Wind direction
Wind speed <sup>a</sup>
Weather Phenomena and Obstructions to Vision
Visibility <sup>a</sup>
Present weather (includes types and intensities of obstructions to vision and precipitation) <sup>a</sup>
Cloud Information
Total cloud cover <sup>a</sup>
Ceiling height (height of that cloud layer above which less than half the sky is observable) <sup>a</sup>
Cloud layer amounts <sup>a</sup>
Cloud layer heights <sup>a</sup>
Cloud layer types

---

<sup>a</sup>Data used in WETTA algorithms.

Solar elevation angle is an additional variable that is an important factor in several of the algorithms. Geographical coordinates, date, and time are all that are needed to calculate solar elevation angle.

### III. WETTA MODEL ALGORITHMS

There are a number of target acquisition models for visual and infrared systems [1,2,5-9], and, although they differ somewhat in form and complexity, they all have to contend (at least implicitly) with the same sets of weather conditions and phenomena that affect the transmission of image information from target scene to sensor. I have isolated these universal weather factors from the other factors involved in target acquisition modeling. My method for estimating the values of the relevant atmospheric parameters is, therefore, independent of any specific target acquisition model.

The relationships between atmospheric parameters and target acquisition system performance are complicated. The effects of the different atmospheric parameters are interactive; they cannot be calculated separately and then simply combined, either for a single type of acquisition system or for different types of systems. The atmospheric parameters themselves are correlated and, hence, cannot be treated statistically as independent variables. Finally, the parameters are highly variable in space and time; system performance is apt to be similarly variable, which, in turn, could have important implications in weapon-mix deployments and in weapon use concepts.

The main problem, then, is to use a source of weather information in which as much as possible of the parametric interdependency and space-time variability is intact. The computer-compatible archives of surface weather observations meet these criteria best. In essence, the method creates a vertical-profile "model" of atmospheric parameters from the information contained in each surface weather observation. These parameters have been put into a target acquisition model to quantify the performance of specific systems against specific targets in the climates depicted by selected sequences of historical weather data.

In developing the algorithms, I have focused on the visible and 8-12  $\mu\text{m}$  infrared portions of the electromagnetic spectrum, for these are the principal wavelength regions currently being exploited for imaging sensors. The image-transmission related parameters estimated

from surface weather observables are grouped according to spectral region.

Visible Image Transmission

1. Visible extinction coefficient
2. Sky-ground ratio

8-12  $\mu\text{m}$  Infrared Image Transmission

3. 8-12  $\mu\text{m}$  extinction coefficient
  - a. Water vapor molecular absorption coefficient
  - b. Water vapor continuum absorption coefficient
  - c. Aerosol extinction coefficient

Both Visible and Infrared Transmission

4. Cloud-free line of sight
5. Atmospheric vertical structure

VISIBLE EXTINCTION COEFFICIENT

"Visibility" is the routinely observed surrogate for the visible extinction coefficient. Visible transmission is affected by all atmospheric aerosols (haze, smoke, smog, fog, etc.). The Koschmieder visibility theory [10] defines the relationship,

$$V = \frac{1}{\beta} \ln \frac{1}{C_t},$$

where  $V$  is the maximum range at which an ideal black target can be seen against the horizon (the "visibility"),  $\beta$  is the visible extinction coefficient, and  $C_t$  is the observer's threshold contrast (the contrast at which 50 percent of all observers would see the target). Middleton [11] discusses at length the practical problems in using this equation to estimate  $\beta$  from observations of  $V$ . Visibility is estimated by observers having different threshold contrasts using nonstandard arrays of nonideal visibility targets.

Koschmieder assumed  $C_t = 0.02$ , whence

$$V = \frac{3.912}{\beta},$$



which has become adopted as a sort of "standard" and been given various names, such as "meteorological range," to distinguish it from observed visibility. Measurements by Hering [12] strongly support the  $C_t = 0.02$  value for ideal visibility estimating conditions (a carefully placed array of large black markers), but the effective value of  $C_t$  increased rapidly when natural markers beyond the array were used. Middleton reports two comparisons of contrast measurements against visibility observations under field conditions, resulting in mean effective threshold contrasts of 0.031 and 0.039. This, plus a smattering of additional evidence also reported by Middleton, leads me to adopt the value  $C_t = 0.035$  as a statistically representative bridge between reported visibilities and actual extinction coefficients; therefore, for present purposes,

$$\beta \approx \frac{3.352}{V}.$$

If  $V$  is km, the units for  $\beta$  are neper  $\text{km}^{-1}$  (the neper is the natural logarithmic analog of the decibel). The difference between these two assumptions for  $C_t$  is shown in Fig. 1. The use of  $C_t = 0.035$  results in the inferred visible extinction coefficient being 15 percent lower than with  $C_t = 0.02$ .

#### SKY-GROUND RATIO

Visual image transmission is formulated as target-to-background *contrast* transmission, per Duntley [13]. His algebraic formulation makes use of the ratio of the luminance of the horizon sky ( $L_s$ ) to the luminance of the ground near the target ( $L_g$ ), both taken in the azimuth toward the target, the so-called "sky-ground ratio."<sup>1</sup> It arises, physically, because of extraneous light being scattered into the sensor field of view by atmospheric aerosols. The received contrast at range

---

<sup>1</sup>Some researchers prefer the use of a closely related variable, "directional path reflectance," in lieu of the "sky-ground ratio." The preference, in my opinion, is arbitrary, for both involve similar problems in measurement or approximation. For backgrounds and targets whose luminances consist entirely of reflected light, their *reflectances* can be used in place of their luminances; and we do so commonly when dealing with military target detection in daylight.

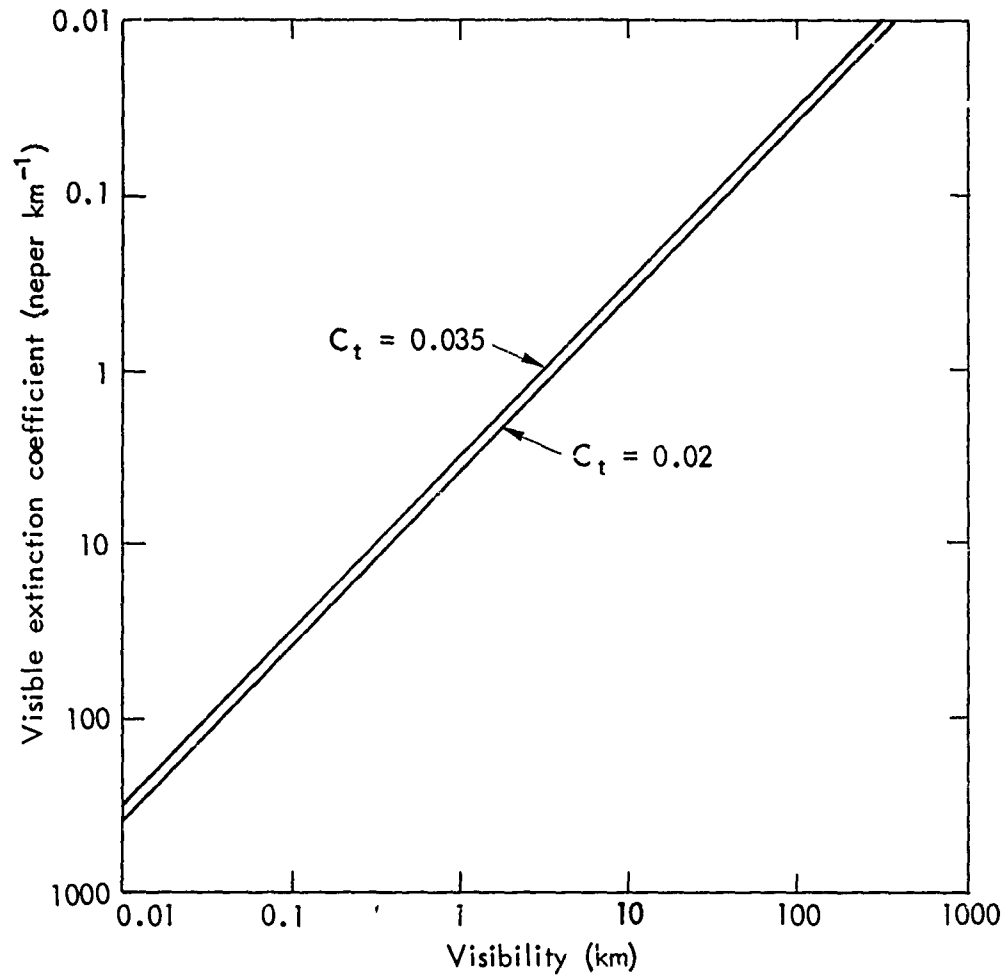


Fig. 1—Visibility versus extinction coefficient for two assumed values of threshold contrast ( $C_t$ )

$R$ ,  $C_R$ , is related to the inherent (near zero range) target-to-background contrast,  $C_0$ , and the visible extinction coefficient,  $\beta$ , by

$$C_R = C_0 \left[ 1 + \frac{L_s}{L_g} (e^{\beta R} - 1) \right]^{-1}.$$

$L_s/L_g$ , the sky-ground ratio, cannot simply be calculated on physical principles; it varies complexly with geometry (relative positions of

sun, observer, and target), extinction coefficient (visibility), cloud conditions, and surface albedo (which I take to be the same as background luminance). There is no rigorous analytical way to calculate  $L_s/L_g$  from weather data; therefore, a purely empirical method is used, based on calculations given in Duff [14] who used both radiometric measurements (by Duntley et al. [15] in Southern Germany) and the RRA/AFCL model of multiple scattering in the atmosphere [16]. A detailed examination of Duff's calculations permits the following generalizations to be drawn: The sky-ground ratio

- (a) increases with decreasing surface albedo;
- (b) increases with decreasing visibility;
- (c) increases with decreasing solar elevation angle;
- (d) is independent of sun angle under cloudy skies;
- (e) is maximum with receiver depression angle (look angle) 10-30°;
- (f) is minimum with receiver depression angle near 0° and 50-70°;
- (g) has maximum value about 2 to 3 times minimum values as a function of receiver depression angle;
- (h) does not depend strongly on azimuth relative to the sun; and
- (i) averages about 2 to 5 in Germany in summer with good visibility.

The sky-ground ratio algorithm produces results in conformity with the above general rules. First, an estimate for sky-ground ratio ( $\hat{SG}$ ) is made independently for each of three of the four variables of which it is a function. These three are the surface albedo ( $\rho$ ), the solar elevation angle ( $\epsilon$ ) and the visibility ( $V$ ). In each case, the shape or trend of the functional relationship as calculated by Duff is not violated, and values are reproduced that are consistent with those that correspond to a receiver depression angle ( $\delta$ ), the fourth variable, between about 80° and 50°. These independent estimates are averaged and then multiplied by a factor ( $F_\delta$ ) that accounts for the dependence of

$L_s/L_g$  on  $\delta$ , the form of which varies as a function of the first three variables. Hence, a sky-ground ratio estimate,  $\hat{SG}$ , is calculated as follows:

$$L_s/L_g \approx \hat{SG} = F_\delta (\hat{SG}_\rho + \hat{SG}_\epsilon + \hat{SG}_V)/3,$$

where

$$\hat{SG}_\rho = \exp (-1.15 \ln \rho - .75),$$

$$\hat{SG}_\epsilon = \exp (-3.4 \sin \epsilon + 2.7),$$

$$\hat{SG}_V = \exp (-.5 \ln V + 1.5).$$

If the sky is broken or overcast (cloud amount  $> 4/8$ ),  $\epsilon$  is set at  $25^\circ$ . Curves for the three expressions for  $\hat{SG}$  are plotted as solid curves in Fig. 2. The dashed curves on Figs. 2a and 2b are Duff's calculations from the RRA/AFCRL multiple-scattering model for values of the other variables that more or less bound my approximation. The curve with open circles on Fig. 2a is a long-standing approximation (due to Duntley as reported by Middleton [11]) of sky-ground ratio as a function of surface albedo;  $\hat{SG}_\rho$  is a compromise between Duff's calculations and Duntley's suggested approximation. As far as the visibility function

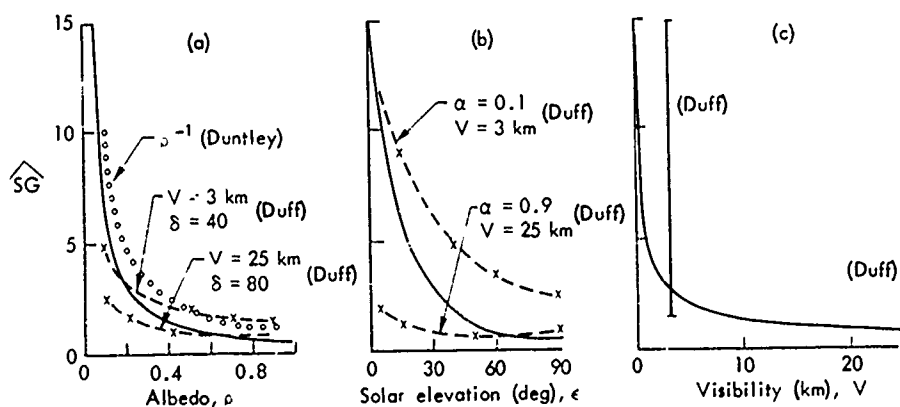


Fig. 2—Independent estimates of sky-ground ratio ( $\hat{SG}$ ) from (a) surface albedo, (b) solar elevation angle, and (c) visibility with other estimates and calculations shown for reference purposes.

is concerned (Fig. 2c), very little information was available on which to base any functional relationship, because Duff's calculations were for only two visibilities, 3 km and 24 km, resulting in ranges of values for sky-ground ratio as shown by the vertical bars.

The factor  $F_\delta$  is calculated as in Tables 3 and 4, which were constructed empirically from examination of many plots (from Duff's calculations) of  $L_g/L_g$  vs  $\delta$  for different combinations of  $\epsilon$ ,  $\rho$  and  $V$ . To use these tables, first determine values of indices  $j_1$ ,  $j_2$ ,  $j_3$ , and  $j_4$  from the assumed or calculated values of  $\delta$ ,  $\epsilon$ ,  $\rho$ , and  $V$  as in Table 3. Then, in Table 4, the appropriate value of  $F_\delta$  is found opposite the resulting combination of  $j$ -index values. Figure 3 shows sample plots of sky-ground ratio (as calculated by the multiple-scattering model) versus receiver depression angle,  $\delta$ , for two visibilities, two albedos, two sun angles, and overcast skies. Also plotted are data points, dots (averages), and vertical bars (ranges of values) for four measurement flights over Southern Germany, for which  $\rho \approx .1$ ,  $35^\circ < \epsilon < 50^\circ$ , and  $7 \text{ km} < V < 30 \text{ km}$ . The horizontal dotted lines on Fig. 3 represent algorithm calculations,  $\hat{S}G$ , that correspond to values of the variables for which the uppermost dashed curve was calculated by the multiple-scattering model ( $\rho = .1$ ,  $\epsilon = 20^\circ$ ,  $V = 25 \text{ km}$ ). The difference between the two estimates is mainly because  $\hat{S}G_\rho$  gives, at small values of  $\rho$ , a sky-ground ratio estimate that is greater than that estimated by the multiple-scattering model. Finally, the open circles on the vertical bars are algorithm calculations for the approximate average of conditions encountered by the measurement flights over Southern Germany ( $\rho = .1$ ,  $\epsilon = 43^\circ$ ,  $V = 18 \text{ km}$ ).

#### 8-12 $\mu\text{m}$ EXTINCTION COEFFICIENT

The total atmospheric extinction coefficient for 8-12  $\mu\text{m}$  radiation can be taken, to a good approximation, to be the sum of a water vapor molecular absorption coefficient ( $\gamma_m$ ), a water vapor continuum absorption coefficient ( $\gamma_c$ ), and an aerosol extinction coefficient ( $\gamma_a$ ). The first two are functions of absolute humidity; the second is also a function of temperature.

Table 3

VALUES OF INDICES  $j_1, j_2, j_3, j_4$  AS FUNCTIONS OF  $\delta, \epsilon, \rho, V$

$j_1$	$\delta$ (deg)	$j_2$	$\epsilon$ (deg)	$j_3$	$\rho$	$j_4$	$V$ (km)
1	$\delta \geq 82$	1	$\epsilon \leq 10$	1	$\rho \geq .5$	1	$V \geq 10$
2	$50 > \delta \geq 30$	2	$10 < \epsilon \leq 30$	2	$.5 > \rho \geq .15$	2	$10 > V$
3	$30 > \delta \geq 12$	3	$30 < \epsilon \leq 55$	3	$.15 > \rho$		
4	$12 > \delta$	4	$55 < \epsilon$				

Table 4

VALUES OF  $F_\delta$  AS FUNCTION OF INDICES  $j_1, j_2, j_3, j_4$ <sup>a</sup>

$j_1$	$j_2$	$j_3$	$j_4$	$F_\delta$	$j_1$	$j_2$	$j_3$	$j_4$	$F_\delta$	$j_1$	$j_2$	$j_3$	$j_4$	$F_\delta$	$j_1$	$j_2$	$j_3$	$j_4$	$F_\delta$
1	1	1	1	2	2	1	1	1	1	3	1	1	1	1.2	4	1	1	1	1.2
1	1	1	2	2	2	1	1	2	1.2	3	1	1	2	2	4	1	1	2	0.8
1	1	2	1	2	2	2	1	2	1	3	1	2	1	1.5	4	1	2	1	1.5
1	1	2	2	2	2	2	1	2	1.2	3	1	2	2	2.5	4	1	2	2	1
1	1	3	1	2	2	2	1	3	1.2	3	1	3	1	2.5	4	1	3	1	2.5
1	1	3	2	2	2	2	1	3	2	3	1	3	2	3.5	4	1	3	2	1
1	2	1	1	1.5	2	2	1	1	1	3	2	1	1	1.2	4	2	1	1	1.2
1	2	1	2	1.5	2	2	1	2	1.2	3	2	1	2	1.7	4	2	1	2	0.8
1	2	2	1	1.5	2	2	2	1	1	3	2	2	1	1.2	4	2	2	1	1.2
1	2	2	2	1.5	2	2	2	2	1.2	3	2	2	2	2	4	2	2	2	0.8
1	2	3	1	1.5	2	2	3	1	1.2	3	2	3	1	2	4	2	3	1	2
1	2	3	2	1.5	2	2	3	2	1.5	3	2	3	2	3	4	2	3	2	1
1	3	1	1	1.5	2	3	1	1	1	3	3	1	1	1	4	3	1	1	1.2
1	3	1	2	1.5	2	3	1	2	1.2	3	3	1	2	1.2	4	3	1	2	0.7
1	3	2	1	1.5	2	3	2	1	1	3	3	2	1	1.2	4	3	2	1	1.2
1	3	2	2	1.5	2	3	2	2	1.2	3	3	2	2	1.5	4	3	2	2	0.8
1	3	3	1	1.5	2	3	3	1	1.2	3	3	3	1	1.5	4	3	3	1	1.5
1	3	3	2	1.5	2	3	3	2	1.5	3	3	3	2	2	4	3	3	2	0.8
1	4	1	1	1	2	4	1	1	1	3	4	1	1	0.7	4	4	1	1	1
1	4	1	2	1	2	4	1	2	1	3	4	1	2	1	4	4	1	2	0.5
1	4	2	1	1	2	4	2	1	1	3	4	2	1	1	4	4	2	1	1
1	4	2	2	1	2	4	2	2	1	3	4	2	2	1.2	4	4	2	2	0.7
1	4	3	1	1	2	4	3	1	1	3	4	3	1	1	4	4	3	1	1
1	4	3	2	1	2	4	3	2	1.2	3	4	3	2	1.5	4	4	3	2	0.7

<sup>a</sup>For  $82 > \delta \geq 50$ ,  $F_\delta = 1$ .

A useful approximation for absolute humidity near sea level ( $\approx 1000$  mb pressure),  $A'$  ( $\text{gm m}^{-3}$ ), in terms of the dewpoint temperature,  $T_d$  ( $^{\circ}\text{F}$ ), is given by

$$\log_{10} A' \approx 0.016 T_d + .16.$$

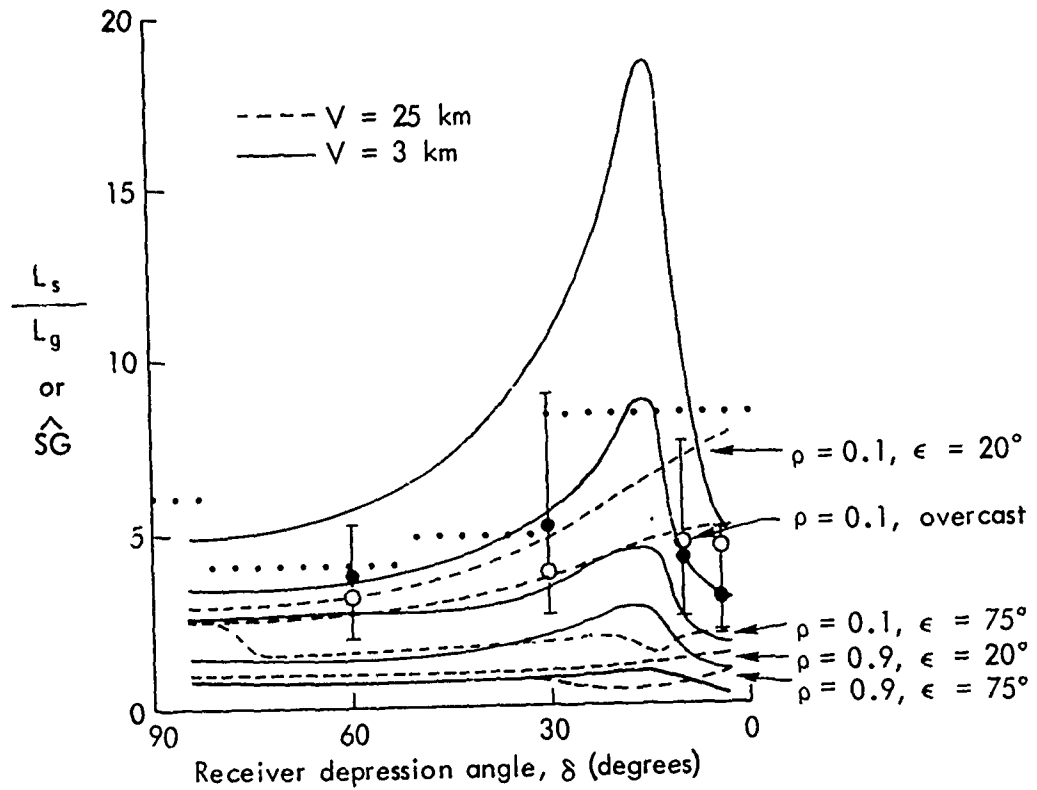


Fig. 3-- Sample values of sky-ground ratio ( $L_s/L_g$ ) calculated by Duff [14] using a multiple-scattering model (solid and dashed curves) and aircraft measurements over Germany (vertical bars). Arrows point toward intersections of the two curves (for different values of  $V$ ) that correspond to the indicated values of  $\rho$  and  $\epsilon$ . Dotted lines and open circles are algorithm calculations,  $\hat{S}\hat{G}$ .

At greater heights up to  $\approx 6000$  m, the absolute humidity,

$$A \approx A' (1 + .0003 Z),$$

where  $A'$  is calculated from the dewpoint at height  $Z$  (m) as if it were the dewpoint at  $Z = 0$  ( $\approx 1000$  mb).<sup>1</sup>

#### Water Vapor Molecular Absorption Coefficient (8-12 $\mu$ m)

McClatchey et al. [17] give graphical methods by which the two types of water vapor ( $H_2O$ ) absorption coefficients,  $\gamma_m$  and  $\gamma_c$ , can be estimated from the absolute humidity. The basis of these methods has also been incorporated by Selby and McClatchey into a computer program for atmospheric transmittance over the wavelength range 0.25 - 28.5  $\mu$ m, the latest published version of which is LOWTRAN 3 [18].

A curve fit to the average  $H_2O$  molecular absorption coefficient over 8-12  $\mu$ m calculated by the method of Ref. 17 gives

$$\log_{10} \gamma_m \approx .58 \log_{10} A - 1.75.$$

#### Water Vapor Continuum Absorption Coefficient (8-12 $\mu$ m)

When the method of Ref. 17 is used to calculate  $H_2O$  continuum absorption coefficients for 8-12  $\mu$ m radiation, over consistent combinations of temperatures from 22 to 94°F and pressures from 1000 to 800 mb, a reasonable linear fit is given by

$$\gamma_c(\text{Ref. 17}) \approx .01432A.$$

Roberts, Biberman, and Selby [19] have suggested corrections to the Ref. 17 method for  $\gamma_c$ , based upon their examination of a large number of more recent atmospheric and laboratory measurements. First, they suggest an approximate 25 percent reduction in the 8-12  $\mu$ m  $\gamma_c$  calculated by the older method and state that the corrected value should

---

<sup>1</sup>Approximations for absolute humidity derived from basic hygrometric formulas.  $A'$  is accurate within 5 percent in the dewpoint range 10°F - 70°F.



be valid at 296°K (73°F). They further suggest a strong temperature dependence of  $\gamma_c$ . (These corrections have been accepted by the designers of the computer model LOWTRAN 3, and are incorporated into a revision, LOWTRAN 3A). The resulting approximate value is given by

$$\gamma_c \approx .01074A \exp \left\{ 1800 \left[ \frac{1}{\frac{5}{9} T + 255.4} - \frac{1}{296} \right] \right\},$$

where T is temperature in °F.

A graphical summary of these approximations for both types of H<sub>2</sub>O absorption coefficients is presented in Fig. 4. "X" plots and the vertical bars indicate, respectively, values calculated for  $\gamma_m$  and ranges of values calculated for  $\gamma_c$  by the graphical method of Ref. 17; and the associated curves are produced by approximating expressions. The solid curves for  $\gamma_c$  incorporate the corrections of Ref. 19, and are terminated at the point where the combinations of absolute humidity and temperature are equivalent to 100 percent relative humidity. The corrections of Ref. 19 are incorporated exactly as suggested by the authors of that report; therefore, any discrepancy between my approximations and LOWTRAN 3A calculations should be due to my original approximations to the Ref. 17 method.

#### Aerosol Extinction Coefficient (8-12 $\mu$ m)

Infrared transmission is attenuated by atmospheric aerosols through both scattering and absorption. Aerosol extinction (scattering plus absorption) is a strong function of particle size relative to the wavelength of the radiation, with significant extinction occurring, in general, only if particle radii are of the same order of magnitude as, or larger than, the wavelength. As a result, the IR aerosol extinction coefficient is about two orders of magnitude smaller than the visible extinction coefficient in small-particle aerosols (such as a dry continental haze), but is about equal to the visible extinction coefficient in large-particle aerosols (such as heavy fog, clouds, and precipitation).

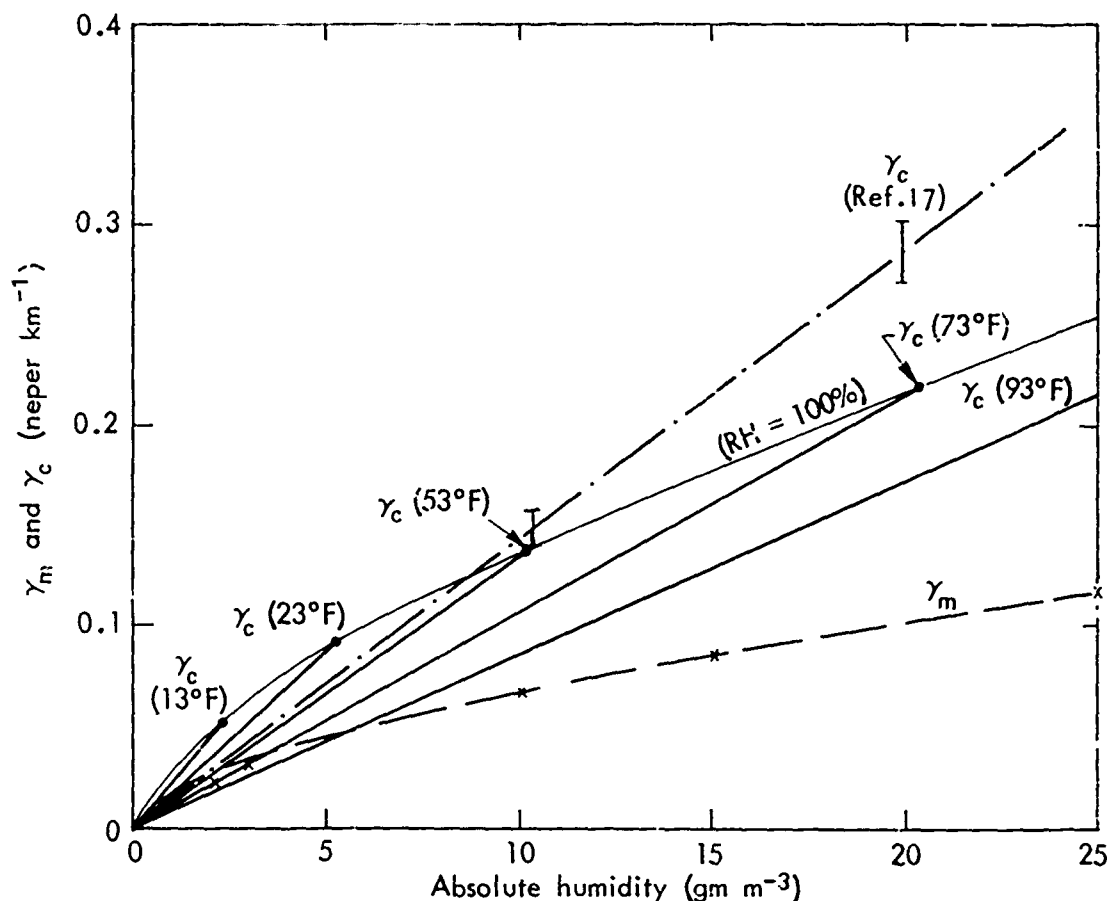


Fig. 4—Approximations for  $\text{H}_2\text{O}$  molecular ( $\gamma_m$ ) and continuum ( $\gamma_c$ ) absorption coefficients for 8-12  $\mu\text{m}$  radiation

A very simple algorithm has been developed to approximate the complex effects of atmospheric aerosols on 8-12  $\mu\text{m}$  transmission. Aerosol particle size, a major governing factor, is a strong function of relative humidity (RH); and the rate at which a particle grows with increasing RH depends, further, on its chemical composition and initial size (see, e.g., Orr et al. [20]; Koenig [21]; Hänel [22]). In general, size increases per incremental increase in RH are small with RH less than about 60-75 percent, and the growth rate increases in an exponential manner at higher RH to about double in radius at 90-95 percent RH and about quadruple in radius at  $\text{RH} \approx 99$  percent. As particles grow

with increasing RH, the aerosol extinction coefficient at 8-12  $\mu\text{m}$ . ( $\gamma_a$ ) should increase more rapidly than the visible extinction coefficient ( $\beta$ ); also, the ratio  $\gamma_a/\beta$  should be expressible, to a first approximation, as a function of RH.

Several investigators have shown that  $\gamma_a/\beta \approx 1$  in fogs, clouds and precipitation, all of which are phenomena associated with  $\text{RH} \approx 100$  percent (see, e.g., Deirmendjian [23,24]; Ruppersberg, Schellhase, and Schuster [25]; Rensch and Long [26]). Estimates of the ratio  $\gamma_a/\beta$  in "dry" atmospheric aerosols ( $\text{RH} < \approx 50$  percent) are much more difficult to find. I have assumed that Deirmendjian's extinction coefficient calculations for his continental "Haze L" particle size distribution model are representative, in general, of dry atmospheric aerosols. Based thereon, my assumption is that  $\gamma_a/\beta \approx .015$  for  $\text{RH} \leq 50$  percent. I have further assumed that Deirmendjian's maritime "Haze M" distribution is generally representative of aerosols with  $\text{RH} \approx 90$  percent; his "Haze M" calculations give  $\gamma_a/\beta \approx .065$  [23]. A function that adequately fits these assumed pairs of RH and  $\gamma_a/\beta$  values is,

for  $50 \text{ percent} \leq \text{RH} \leq 99.5 \text{ percent}$ ,

$$\log_{10} \left( \frac{\gamma_a}{\beta} \right) = -.91 \log_{10} (100 - \text{RH}) - .284.$$

For  $\text{RH} < 50$  percent,

$$\frac{\gamma_a}{\beta} \approx .015;$$

and for  $\text{RH} > 99.5$  percent, or when precipitation is falling,

$$\frac{\gamma_a}{\beta} \approx 1.0.$$

This set of functions is illustrated in Fig. 5.

#### CLOUD-FREE LINE OF SIGHT

Table 5, adapted from Rapp and Schutz [27], is used to estimate the probability of a cloud-free line of sight,  $P_{\text{CFLOS}}$ , as a function

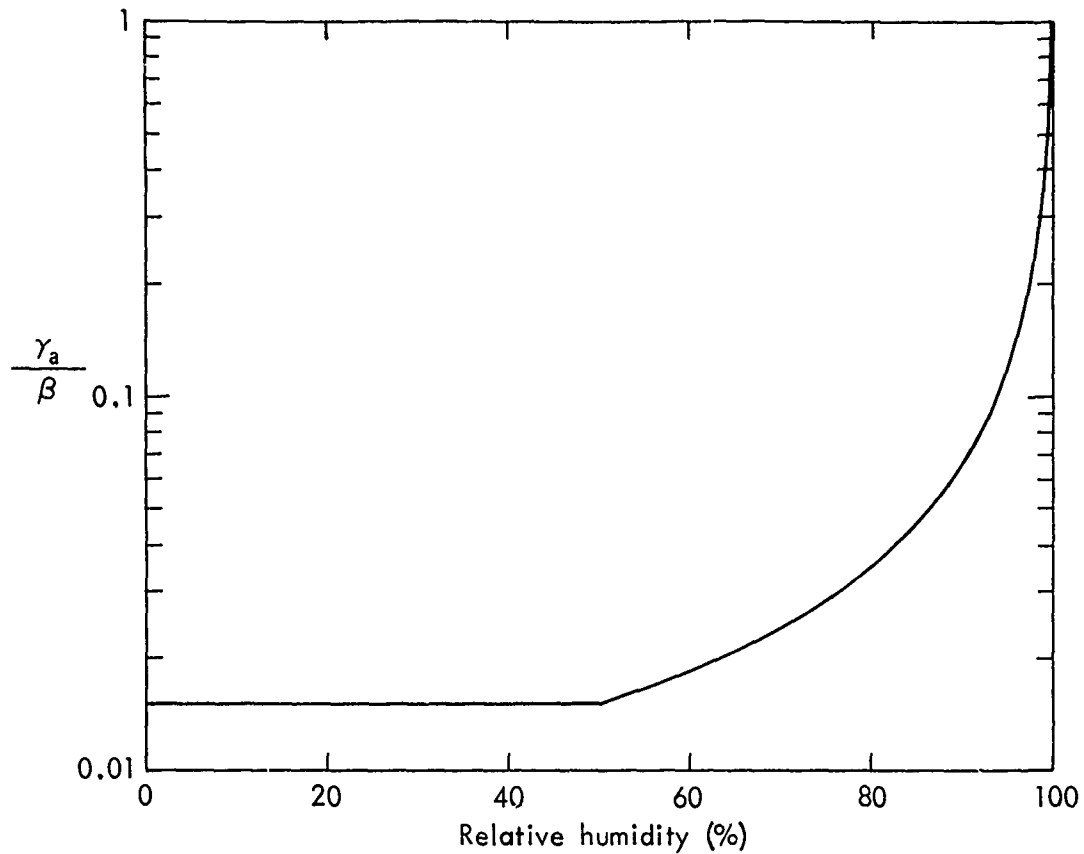


Fig. 5—Assumed function relating  $\gamma_a/\beta$  to relative humidity

of sensor depression angle,  $\delta$ , and total cloud amount,  $N(8\text{ths})$ , in all cloud layers between the sensor altitude and the ground. The original data for  $P_{\text{CFLOS}}$  are those of Shanklin and Landwehr [28], which Rapp and Schutz aggregated by averaging over all line-of-sight azimuth angles and interpolated for cloud amounts reported in 8ths rather than in 10ths.

All clouds are assumed to be opaque for both visible and 8-12  $\mu\text{m}$  radiation; therefore, for practical application in air-to-ground target acquisition problems, their *principal* effect is to limit the maximum altitude of air-to-ground systems.

#### ATMOSPHERIC VERTICAL STRUCTURE

Aircraft measurements of visible extinction coefficients in the atmosphere by Duntley et al. [11,29-31] give strong support to the view

Table 5

PROBABILITY OF A CLOUD FREE LINE OF SIGHT ( $P_{CFLOS}$ )  
AS A FUNCTION OF SENSOR DEPRESSION ANGLE ( $\delta$ ) AND  
INTERVENING CLOUD AMOUNT (N)

N (8ths) as Reported by Ground-based Weather Observers									
$\delta^a$	0	1	2	3	4	5	6	7	8
0 <sup>b</sup>	(.94)	(.78)	(.63)	(.48)	(.36)	(.27)	(.18)	(.09)	(0)
10	.96	.85	.71	.59	.46	.36	.27	.15	.01
20	.97	.90	.80	.68	.58	.48	.36	.21	.03
30	.98	.92	.85	.76	.66	.55	.43	.26	.05
40	.99	.93	.88	.80	.68	.59	.47	.30	.07
50	.99	.94	.89	.82	.74	.64	.50	.33	.08
60	1.00	.95	.90	.83	.76	.67	.53	.34	.08
70	1.00	.95	.90	.84	.77	.68	.54	.35	.08
80	1.00	.95	.90	.84	.77	.69	.54	.35	.08
90	1.00	.95	.90	.84	.77	.69	.55	.35	.08

<sup>a</sup>Linear interpolation in  $\delta$  and N is permissible. N will normally be an integer from 0 to 8.

<sup>b</sup>Use  $\delta = 0$  row only for interpolating between  $\delta = 0$  and  $\delta = 10$ . For a surface-to-surface look-path ( $\delta = 0$ ),  $P_{CFLOS} \equiv 1.00$ .

that non-cloud aerosols (dust and other particulate pollutants) are usually homogeneously distributed throughout a well-mixed layer of the atmosphere that extends from the earth's surface to about 1500 m,  $\pm$  1000 m, approximately, depending on the gross stability characteristics of the atmosphere at the given time and place. Of 26 extinction coefficient profiles measured over Southern Germany, Illinois, and New Mexico, 22 clearly show a homogeneous boundary layer with extinction coefficient very near the surface value, above which an apparently typical upper-atmosphere extinction coefficient of  $0.02 - 0.06 \text{ neper km}^{-1}$  usually prevails. Because of this and other considerations, I have adopted a layered, rather than exponential, model of vertical atmospheric structure.

The number of layers, layer dimensions, and physical characteristics are deduced from surface weather observables by the decision tree shown in Fig. 6. The determining parameters, all strongly associated with the static stability of the lower atmosphere, are precipitation

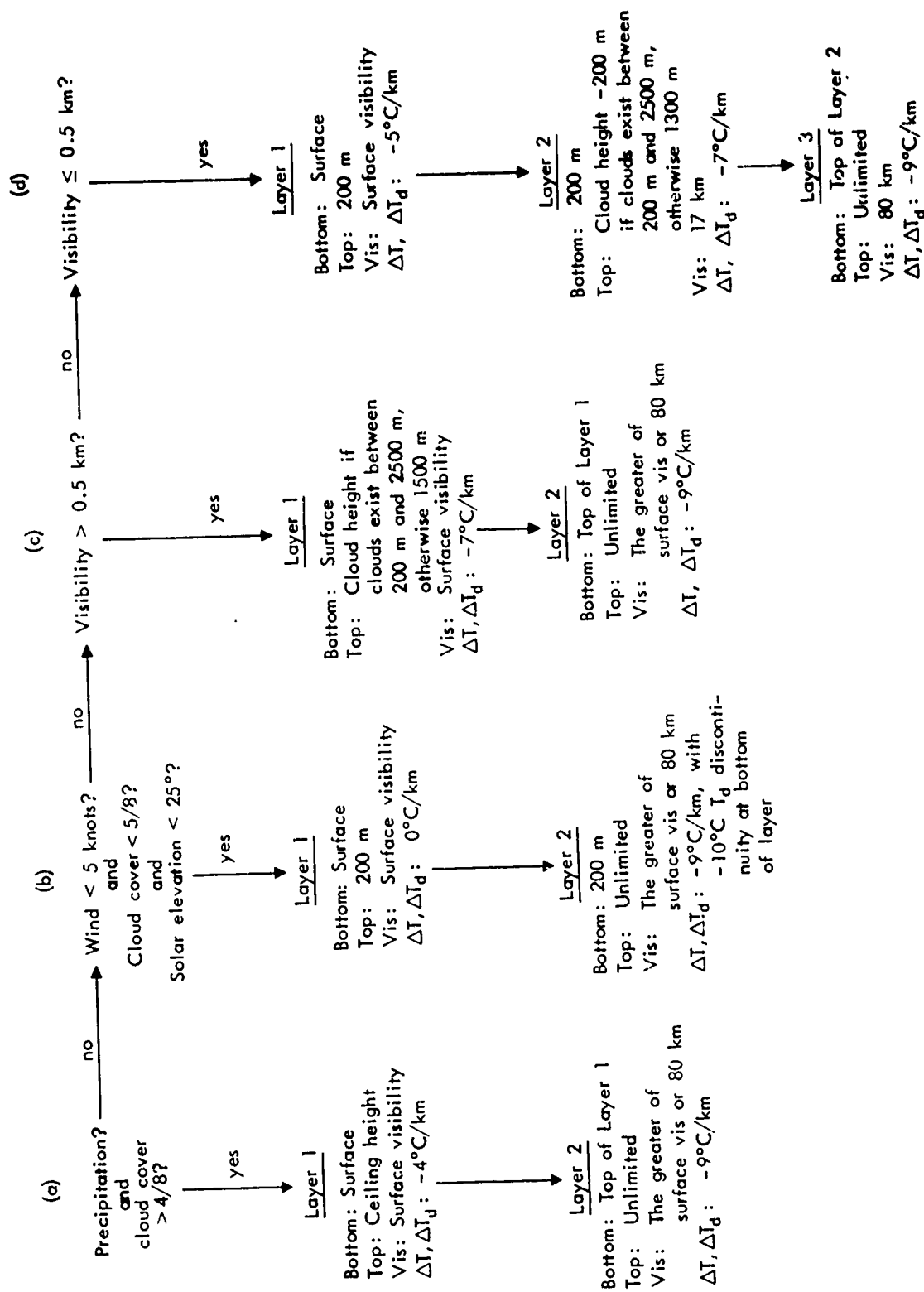


Fig. 6—Decision tree for inferring vertical structure from surface weather data

(whether or not occurring), cloud amount, wind speed, visibility, and solar elevation angle. Four basic vertical structure "models" are used in which the atmosphere is divided into two or three layers of variable thicknesses. The layer properties pertain only to *cloud-free* portions of the layers. The layers are horizontally homogeneous, and every layer is vertically homogeneous in its aerosol extinction properties. Temperature and dewpoint lapse rates (rates of decrease with altitude),  $\Delta T$  and  $\Delta T_d$ , from which absolute and relative humidities are calculated, vary according to atmospheric stability inferences. The lowest layer always has the surface visibility (visible extinction coefficient), and the temperature and dewpoint profiles are always "anchored" by their surface values. The following are brief descriptions of the four basic structures:

(a) When precipitation is falling, the lower layer extends to the base of the precipitating clouds. An upper layer is defined that pertains to the cloud-free air between and above the precipitating clouds (this is nearly irrelevant for visible and IR systems since, by fiat, precipitation from scattered clouds is not treated as a "precipitation" case).

(b) Conditions of light wind, few clouds, and low (or no) sun indicate a stable surface layer, which is given an arbitrary depth of 200 m. The single upper layer has excellent visibility and is made much drier than the lower layer by imposing a 10°C dewpoint discontinuity at the interlayer boundary.

(c) When above conditions are not met, a neutral or unstable atmosphere is indicated; and if visibility does not indicate a heavy fog or local heavy pollution, a lower mixed layer is assumed with depth equal to the height of the lowest cloud layer ( $\leq 2500$  m and  $> 200$  m) or, by default, 1500 m. The upper layer has excellent visibility. There is no dewpoint discontinuity at the interlayer boundary as in (b), above.

(d) With all conditions as in (c), above, except visibility  $\leq 0.5$  km, it is assumed that there is a lower layer of fog or pollution (200 m depth) and a middle layer with fairly good visibility (17 km). The depth of the middle layer and all characteristics of the uppermost layer are calculated as in the two layers in the type (c) structure.

The atmospheric vertical structure models thus defined for each surface weather observation contain all the physical variables and spatial dimensions needed to calculate the atmospheric transfer functions of visible contrast and IR signal-to-noise ratio along any specified or calculated line of sight. It is important to be aware that the assumption of horizontal homogeneity and the simplistic depiction of elevated layers restricts the applicability of the model to target acquisition at short ranges and low altitudes (say, < 20 km range and < 5000 m altitude).



#### IV. NEEDS FOR IMPROVEMENT

This work has made clear the need for improved understanding in a number of areas:

- o *Sky-ground ratio,  $L_s/L_g$ .* Duff's calculations of sky-ground ratio [14] are unique. Atmospheric transfer of visual contrast appears to be so sensitive to this parameter (see Fig. 7) that more measurements and theoretical calculations are warranted.

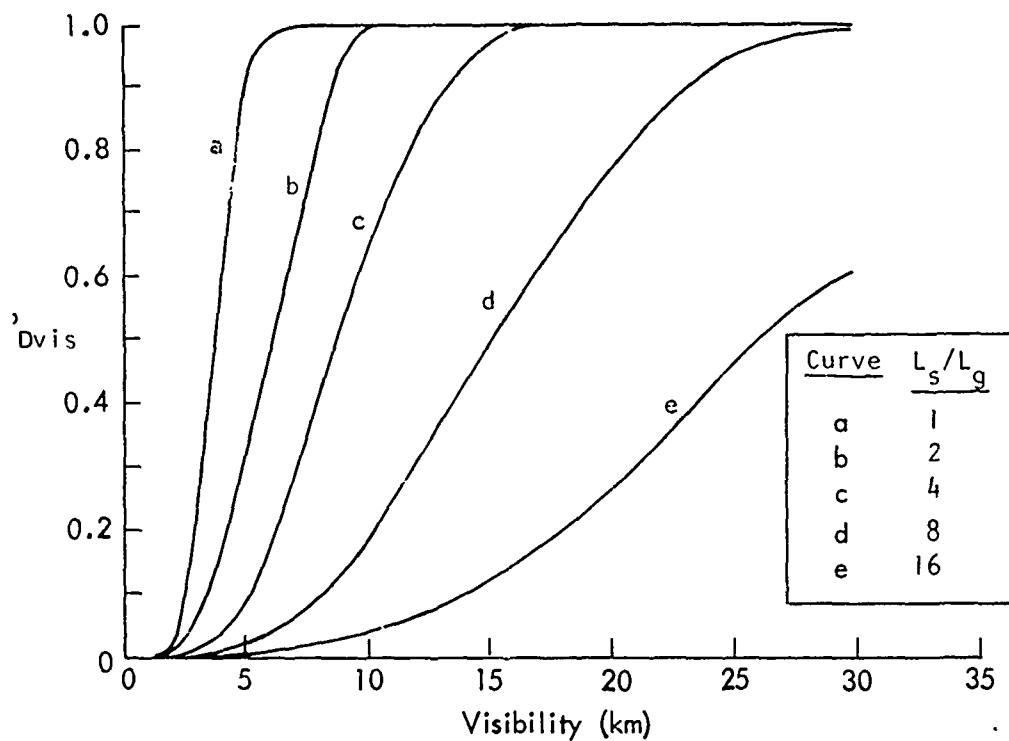


Fig. 7—Calculated visual target detection probability ( $P_{D \text{ vis}}$ ) as a function of visibility for different value of sky-ground ratio ( $L_s/L_g$ ). Characteristic target dimension is 3m and inherent contrast is 0.4.

- o *8-12  $\mu\text{m}$  aerosol extinction coefficient,  $\gamma_a$ .* My scheme to scale this parameter as a function of visible extinction coefficient (visibility) and relative humidity is tentative and simplistic, but is in the right direction. In recent tests of IIR seekers in Germany, serious image degradation was consistently noted coincident with low visibility and high relative humidity [32,33]. My algorithm says, in effect, that dry hazes, smokes, etc. contain mainly small particles that degrade visible transmissions much more than IR transmission, and that very wet aerosols ( $\text{RH} \rightarrow 100$  percent) contain enough large particles that have grown through accretion of water that IR degradation approaches visible degradation. I have set aside, at least for the present, some potentially important differences among aerosols of different origins (sea salt, continental dust, forest fire smoke, industrial effluents, etc.), such as different "dry" size distributions, different growth rates with relative humidity, and different spectral absorptivities. In the context of my modeling approach--statistically valid modeling from surface weather data--I do not know if these differences would be significant. Perhaps each major generic type of aerosol should be represented by its own scaling function for  $\gamma_a$ ; the decision as to which aerosol type exists would then have to be based on geographical and meteorological criteria.

There are also miscellaneous uncertainties in deducing atmospheric vertical structure and CFLOS probability, but I consider these to be unimportant compared with the above problems and compared with the following questions, which have hardly been addressed at all in the context of target detection:

- o *Effects of aerosol infrared emissions.* Carlon [34,35] has suggested that emissions of atmospheric aerosols at infrared wavelengths can be a major factor in reducing the received contrast of thermal images. Absorption by liquid water is

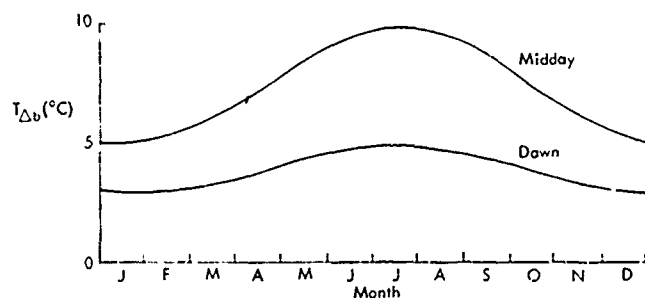
strong in the 8-12  $\mu\text{m}$  region; thermal emission by the absorber will be correspondingly strong, but most important, the wavelength of maximum emission intensity for a black body at typical ambient air (and aerosol) temperatures ( $\approx 285^\circ\text{K}$ ) is near 10  $\mu\text{m}$ . One would expect, therefore, that when a water aerosol is present (nominally at  $\text{RH} > \approx 60$  percent, especially at  $\text{RH} \rightarrow 100$  percent) the atmosphere would "glow" in the 8-12  $\mu\text{m}$  band and have a degrading effect on IR image contrast transmission that is similar to the effect of scattered "airlight" or "path luminance" (parameterized by the sky-ground ratio) on the transmission of visual image contrast.

- o *Weather effects on the target scene.* This problem encompasses both visible and IR depictions of the target scene, but I pass over the visible problems (shadow variations, snow-covered ground, etc.) in favor of the problems associated with deducing the thermal characteristics of the target scene from surface weather data. Batten [36] has suggested a preliminary quantitative algorithm for typical temperature differences found among the natural features of pastoral terrain in north-temperate latitudes, based on season, time of day, and weather conditions. His data sources were two sets of airborne IR radiometer measurements (in Wisconsin [37] and in Germany [38]) and one set of measurements made with tower-mounted radiometers (in New Hampshire) [39]. Batten's algorithm for background thermal clutter,  $T_{\Delta b}$  ( $^\circ\text{C}$ ), is summarized in Table 6 and Fig. 8. None of these basic data sets were acquired with IIR target detection problems in mind, so there could be some important interpretation problems relating to scene content and scale.

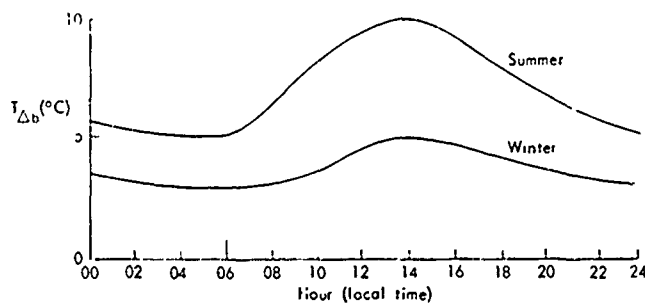
Table 6

VALUES OF BACKGROUND CLUTTER FOR VARIOUS METEOROLOGICAL CONDITIONS

Meteorological Condition	$T_{\Delta b}$ ( $^{\circ}\text{C}$ )
Clear to scattered skies (0 to 4/8)	Seasonal variation given in Fig. 8a for dawn and midday. Diurnal variation for summer and winter given by Fig. 8b.
Broken to overcast skies ( $> 4/8$ to 8/8)	Use dawn values given in Fig. 8a.
During precipitation	$1^{\circ}\text{C}$
The 24 hours following precipitation	$3^{\circ}\text{C}$
Snow on ground	$2^{\circ}\text{C}$
Winds greater than 10 knots	Use dawn values given in Fig. 8a.



(a) Seasonal variation of background thermal clutter on clear days



(b) Diurnal variation of background thermal clutter on clear days

Fig. 8—Approximate seasonal and diurnal variations of background thermal clutter,  $T_{\Delta b}$ , for pastoral terrain in north-temperate latitudes with clear skies and low winds

#### V. CONCLUDING REMARKS

The foregoing algorithms were developed for the primary purpose of *statistically valid prediction of visible and 8-12  $\mu$ m transmission properties of the atmosphere in a variety of climates* (different locations and seasonal and diurnal variations). Computationally, the algorithms are fairly simple because, to attain the goal of statistical validity, it is necessary to perform calculations on very large numbers of past surface weather observations. To date, however, the model has been applied only to selected small samples of data.

The methodology described in this report clears the way for the application of historical weather-data sets to the evaluation of multi-spectral "seeing" conditions for almost any location in the world. The algorithms undoubtedly could be improved. It is gratifying to note, in this regard, that most new programs for measuring **atmospheric optical** and image-transmission properties (e.g., Moulton [33], Fenn [40], and Hubbard [41]) include the collection of standard surface weather observations as part of their basic data sets for the specific purpose of correlating the weather observations with the optical measurements.

The methodology could also be expanded to include other portions of the electromagnetic spectrum in which sensors do or might operate. Inclusion of the 3-5  $\mu$ m infrared band would be quite simple. Expansion of the methodology to the near-millimeter and microwave spectral regions, however, would be much more difficult. At those longer wavelengths, clouds cannot be assumed to be opaque, and transmission is a strong function of cloud and precipitation particle size distributions and concentrations. Modeling of these parameters from surface weather observations might be worth attempting, but the uncertainties would be large.

# Appendix A

## TARGET DETECTION MODELING EQUATIONS (AFTER BAILEY AND MUNDIE)

### VISUAL DETECTION EQUATIONS

H. H. Bailey's visual target detection model [1] has been somewhat abbreviated and modified for use with the WETTA algorithms. The main change is that I have not so far used Bailey's "search term" (the probability that an observer, searching the target area, looks for a specified glimpse time in the direction of the target with his foveal vision). Therefore, environmental effects on scene clutter (or congestion) have not been dealt with explicitly as they would affect search time. I have adapted Bailey's "detection term" (the probability that a target is seen given that it is in the observer's foveal field of view) and "resolution term" (the probability that a target is adequately resolved to be recognized--the degree of recognition required can be specified); these are  $P_{Dvis}$  and  $P_{Rvis}$ , respectively, in my nomenclature. The probability of detection with adequate resolution,

$$P_{DRvis} = P_{Dvis} \cdot P_{Rvis}^1$$

$$P_{Dvis} \approx 1/2 \pm 1/2 \sqrt{1 - \exp \left[ -4.2 \left( \frac{C_n}{C_T} - 1 \right)^2 \right]},$$

where " $\pm$ " is "+" for  $C_n/C_t \geq 1$ , "-" otherwise;  $C_n$  is target-to-background contrast transferred through  $n$  atmospheric layers, and  $C_T$  the threshold contrast of the observer-target-range combination.  $C_T$  is defined as the received contrast that yields a 50 percent detection probability, which Bailey has approximated by the hyperbola,

$$\log_{10} C_T \approx (\log_{10} \alpha + 0.5)^{-1} - 2,$$

---

<sup>1</sup>If clouds intervene between target and sensor, then  $P_{DRvis} = P_{CFLOS} \cdot P_{Dvis} \cdot P_{Rvis}$ , where  $P_{CFLOS}$  is probability of a cloud-free line of sight.

where  $\alpha$  is the angular size (minutes of arc) of the small dimension of the target intercepted at the sensor.

$$\alpha \approx 3.44 M\ell/R,$$

where  $M$  is magnification,  $\ell$  is a characteristic (usually minimum projected) dimension of the target (m), and  $R$  is range (km). The received contrast transferred through  $n$  atmospheric layers

$$C_n \approx C_o \prod_{i=1}^n (F_T)_i,$$

where  $C_o$  is inherent target-to-background contrast and  $(F_T)_i$  is contrast "transmittance" (transfer function) through atmospheric layer  $i$ .

$$C_o = \left| \frac{(L_g)_1 - (L_t)_1}{(L_g)_1} \right|,$$

where  $(L_g)_1$  is the background reflectance and  $(L_t)_1$  the target reflectance at the bottom of the lowest atmospheric layer ( $i = 1$ ).

$$(F_T)_i = \left[ 1 + (\widehat{SG})_i (e^{\beta_i R_i} - 1) \right]^{-1},$$

where  $(\widehat{SG})_i$ ,  $\beta_i$  and  $R_i$  are the estimated "sky-ground ratio," visible extinction coefficient (neper  $\text{km}^{-1}$ ), and path length (km), respectively, in atmospheric layer  $i$ . For elevated layers ( $i > 1$ ), sky-ground ratio is calculated from an inferred albedo,  $\alpha_i$ , taken as being equivalent to the background reflectance found at the bottom of that layer, i.e.:

$$\alpha_i = \left| \frac{[(L_g)_{i-1} - (L_t)_{i-1}] e^{-\beta_{i-1} R_{i-1}}}{C_n} \right|,$$

where

$$(L_g)_{i-1} - (L_t)_{i-1} = C_{n-1} \alpha_{i-1}.$$

The "resolution term" (probability of adequate target recognition),

$$P_{Rvis} = 1 - \exp \left\{ - \left[ \left( \frac{1}{\alpha'} \frac{1}{0.4F_s} \right) - 1 \right]^2 \right\},$$

where  $\alpha'$  is required target angular size (minutes, at observer) for a nearly 1.0 probability of seeing the target signal and  $F_s$  is a subjective "shape recognition factor" ranging from 1 (spot recognition; "something is there") to 5 (high confidence shape recognition) by means of which "adequate resolution" is specified.

$$\log_{10} \alpha' = [\log_{10} (2C_T) + 2]^{-1} - 0.5.$$

If

$$\frac{\alpha}{\alpha'} \frac{1}{0.4F_s} \leq 1,$$

then  $P_{Rvis} = 0$ .

The above formulation is for detection by the human eye. In applying it to TV seeker systems, I have implicitly assumed that if the unaided eye can detect a target, then a properly designed TV system and its operator can attain and maintain the necessary lock-on to the target.

#### IIR DETECTION EQUATIONS

The following set of equations for IIR target detection probability is taken from the work of Bailey and Mundie (in Lau et al. [2]). As with the visual detection equations, the probability of detection with adequate resolution,<sup>1</sup>

$$P_{DRir} = P_{Dir} \cdot P_{Rir},$$

where  $P_{Dir}$  is the probability of seeing the target image on the IIR

<sup>1</sup>As noted before, with intervening clouds  $P_{DRir} = P_{CFLOS} \cdot P_{Dir} \cdot P_{Rir}$ .



display given that the target image is in the operator's foveal field of view, and  $P_{Rir}$  is the probability that the target image is adequately resolved for the required degree of recognition.<sup>1</sup>

$$P_{Dir} = 1 - \exp \left[ - \left( \frac{S_n}{N_n} - 1 \right) \right],$$

where  $S_n/N_n$  is the resulting signal-to-noise ratio after image transfer through  $n$  atmospheric layers. If<sup>2</sup>

$$S_n/N_n \leq 1, \quad \text{then} \quad P_{Dir} = 0,$$

$$S_n/N_n = T_{\Delta} \tau_n F_M / T_{\Delta NE},$$

where  $T_{\Delta}$  is target-to-background temperature difference ( $^{\circ}\text{C}$ ),  $\tau_n$  is atmospheric 8-12  $\mu\text{m}$  transmittance through  $n$  atmospheric layers, and  $F_M$  and  $T_{\Delta NE}$  are instrumental modulation transfer function and noise equivalent temperature difference ( $^{\circ}\text{C}$ ), respectively.

$$\tau_n = \prod_{i=1}^n \tau_i,$$

$\tau_i$  being the 8-12  $\mu\text{m}$  transmittance through layer  $i$ , and

$$\tau_i = e^{-R_i(\gamma_m + \gamma_c + \gamma_a)_i},$$

<sup>1</sup>This form for the noise dependence of  $P_D$  is not the only one used.

<sup>2</sup>This equation for  $S/N$  accounts for detector noise, only. The formulation by Rosell and Willson [6] accounts for other noise sources, and also uses the Gaussian form for the equation for  $P_D$ . Comparative calculations (unpublished) by T. F. Lippiatt of The Rand Corporation, using both the above and the Rosell and Willson equations, showed that  $P_D$  predicted by the two methods could be made nearly equivalent by adjustment of a single parameter, display gain, to a value near 5.

where  $R_i$  is path length through atmospheric layer  $i$  and  $\gamma_m$ ,  $\gamma_c$  and  $\gamma_a$  are  $H_2O$  molecular absorption,  $H_2O$  continuum absorption, and aerosol extinction coefficients, respectively, in layer  $i$ .

The probability of adequate target image resolution,

$$P_{Rir} = 1 - \exp \left\{ - \left[ (N_r / 0.4 F_s) - 1 \right]^2 \right\},$$

where  $N_r$  is the number of IIR display resolution lines across the displayed target and  $F_s$  is the shape recognition factor as previously defined; and

$$N_r = \frac{M\ell}{1.19aR},$$

where  $M$ ,  $\ell$ , and  $R$  are the magnification, target dimensions, and range as previously defined, and  $a$  is the angular size (mrad) of the display resolution element. (The factor 1.19 results from applying the Kell factor,  $\sqrt{2}$ , to the vertical resolution element and taking the geometric mean of the size of the vertical and horizontal resolution elements.)

REFERENCES

1. Bailey, H. H., *Target Acquisition Through Visual Recognition: A Quantitative Model*, The Rand Corporation, RM-6158-PR, February 1970.
2. Lau, J., H. H. Bailey, N. W. Crawford, W. H. Krase, M. A. Levin, L. G. Mundie, and D. V. Palmer, *An Analysis of Remotely Manned Systems for Attacking SAM Sites* (U), The Rand Corporation, R-710-PR, September 1971 (Secret).
3. Kelley, C. T., Jr., R. E. Huschke, and C. Schutz, *Weather and PGMs: The Utility of an Adverse Weather Weapon in a NATO Context* (U), The Rand Corporation, R-1763-PR, forthcoming (Secret).
4. Rodriguez, E. and R. E. Huschke, *The Rand Weather Data Bank (RAW-DAB): An Evolving Base of Accessible Weather Data*, The Rand Corporation, R-1269-PR, March 1974.
5. Stathacopoulos, A. D., H. F. Gilmore, and G. Rohringer, *Review of Mathematical Models of Air-to-Ground Target Acquisition Using TV and FLIR Sensors*, General Research Corporation, Santa Barbara (NWC TP 5840, Naval Weapons Center, China Lake), January 1976.
6. Rosell, F. A. and R. H. Willson, *Performance Synthesis of Electro-Optical Sensors*, Westinghouse Defense and Electronic Systems, Baltimore (AFAL-TR-73-260), Air Force Avionics Laboratory, Wright-Patterson Air Force Base, August 1973.
7. Rosell, F. A. and R. H. Willson, *Performance Synthesis of Electro-Optical Sensors*, Westinghouse Defense and Electronic Systems, Baltimore (AFAL-TR-74-104, Air Force Avionics Laboratory, Wright-Patterson Air Force Base), April 1974.
8. Greening, C. P., *Target Acquisition Model Evaluation Final Summary Report*, Autonetics, North American Rockwell (NWC TP 5536, Naval Weapons Center, China Lake), June 1973.
9. Advisory Group for Aerospace Research and Development, NATO, *Aerospace Applications Studies Committee Study No. 5 on Night Vision Devices for Fast Combat Aircraft, Vol. III, Appendix C, TV/IR Comparison Study* (U), AGARD-AR-73, Vol. III, NATO, December 1975 (Secret).
10. Koschmieder, H., "Theorie der Horizontalen Sichtweite," *Beitr. Phys. frein Atmos.*, Vol. 12, 33-53, 171-181, 1924.
11. Middleton, W. E. K., *Vision Through the Atmosphere*, University of Toronto Press, 1952.

12. Hering, W. S., H. S. Muench, and H. A. Brown, *Field Test of a Forward Scatter Visibility Meter*, Environmental Research Paper No. 356, AFCRL-71-0315, Air Force Cambridge Research Laboratories, Bedford, Mass., May 1971.
13. Duntley, S. Q., "The Reduction of Apparent Contrast by the Atmosphere," *J. Opt. Soc. Am.*, Vol. 38, 179, 1948.
14. Duff, E. A., *Atmospheric Contrast Transmission: Application to the Electro-Optical Lock-on Problem*, Masters thesis, Air Force Institute of Technology, Wright-Patterson Air Force Base, June 1972.
15. Duntley, S. Q., R. W. Johnson, and J. I. Gordon, *Airborne Measurements of Optical Atmospheric Properties in Southern Germany*, Visibility Laboratory, UCSD, San Diego (AFCRL-72-0255, Air Force Cambridge Research Laboratories, Bedford, Mass.) July 1972.
16. Wells, M. B., *Contrast Transmission Data for Clear and Hazy Model Atmospheres*, Vols. I, II, III, Radiation Research Assoc., Ft. Worth (AFCRL-68-0660, Air Force Cambridge Research Laboratories, Bedford, Mass.), 1968.
17. McClatchey, R. A., R. W. Fenn, J. E. A. Selby, F. E. Volz, and J. S. Garing, *Optical Properties of the Atmosphere (Third Edition)*, AFCRL-72-0497, Air Force Cambridge Research Laboratories, Bedford, Mass., August 1972.
18. Selby, J. E. A. and R. A. McClatchey, *Atmospheric Transmittance from 0.25 to 28.5  $\mu$ m: Computer Code LOWTRAN 3*, AFCRL-TR-75-0255, Air Force Cambridge Research Laboratories, Bedford, Mass., May 1975.
19. Roberts, R. E., L. M. Biberman, and J. E. A. Selby, *Infrared Continuum Absorption by Atmospheric Water Vapor in the 8-12  $\mu$ m Window*, P-1184, Institute for Defense Analyses, Arlington, Va., April 1976.
20. Orr, C., Jr., F. C. Hurd, and W. J. Corbett, "Aerosol Size and Relative Humidity," *J. Colloid Sci.*, Vol. 13, 472, 1952.
21. Koenig, L. R., *Numerical Modeling of Condensation*, The Rand Corporation, RM-5553-NSF, August 1968.
22. Hänel, G., "The Properties of Atmospheric Aerosol Particles as Functions of the Relative Humidity at Thermodynamic Equilibrium with the Surrounding Moist Air," *Advances in Geophysics*, Vol. 19, 73-188, 1976.
23. Deirmendjian, D., *Electromagnetic Scattering on Spherical Polydispersions*, American Elsevier Publishing Company, New York, 1969.

24. Deirmendjian, D., *Far Infrared and Submillimeter Scattering II: Attenuation by Clouds and Rain*, The Rand Corporation, R-1718-PR, February 1975.
25. Ruppersberg, G. H., R. Schellhase, and H. Schuster, "Calculations about the Transmittance Window of Clouds and Fog at about 10.5  $\mu$ m Wavelength," *Atmos. Environment*, Vol. 9, 723-730, 1975.
26. Rensch, D. B. and R. K. Long, "Comparative Studies of Extinction and Back-scattering by Aerosols, Fog, and Rain at 10.6  $\mu$  and 0.63  $\mu$ ," *Applied Optics*, Vol. 9, 1563-1573, July 1970.
27. Rapp, R. R., C. Schutz, and E. Rodriguez, "Cloud-Free Line-of-Sight Calculations," *J. Appl. Meteorol.*, Vol. 12, 484-493, April 1973.
28. Shanklin, M. D., and J. B. Landwehr, *Photogrammetrically Determined Cloud-Free Lines-of Sight at Columbia Missouri. Final Report*, AFCRL-71-0273, Air Force Cambridge Research Laboratories, Bedford, Mass., April 1971.
29. Duntley, S. Q., R. W. Johnson, and J. I. Gordon, *Airborne and Ground-Based Measurements of Optical Atmospheric Properties in Central New Mexico*, Visibility Laboratory, UCSD, San Diego (AFCRL-72-0461, Air Force Cambridge Research Laboratories, Bedford, Mass.), September 1972.
30. Duntley, S. Q., R. W. Johnson, and J. I. Gordon, *Airborne Measurements of Optical Atmospheric Properties in Southern Illinois*, Visibility Laboratory, UCSD, San Diego (AFCRL-TR-73-0422, Air Force Cambridge Research Laboratories, Bedford, Mass.), July 1973.
31. Duntley, S. Q., R. W. Johnson, and J. I. Gordon, *Airborne and Ground-Based Measurements of Optical Atmospheric Properties in Southern Illinois*, Visibility Laboratory, UCSD, San Diego (AFCRL-TR-74-0298, Air Force Cambridge Research Laboratories, Bedford, Mass.), June 1974.
32. Biberman, L. M. and G. A. duMais, *Modeling the Effects of Weather on 8.5 - 11 Micrometer FLIR Performance*, Institute for Defense Analysis, paper presented at Target Acquisition Symposium, U.S. Army Night Vision Laboratory, Ft. Belvoir, June 1976.
33. Moulton, J. R., *European Atmospheric Optical Environment*, U.S. Army Night Vision Laboratory, paper presented at Target Acquisition Symposium, U.S. Army Night Vision Laboratory, Ft. Belvoir, June 1976.
34. Carlon, H. R., "Infrared Emission by Fine Water Aerosols and Fogs," *Appl. Optics*, Vol. 9, 2000, September 1970.
35. Carlon, H. R., "Model for Infrared Emission of Water Vapor/Aerosol Mixtures," *Appl. Optics*, Vol. 10, 2297, October 1971.

37. Lenschow, D. H. and J. Dutton, "Surface Temperature Variations Measured from an Airplane over Several Surface Types," *J. Appl. Meteorology*, Vol. 3, No. 1, 65-69, 1964.
38. Lorenz, D., "Temperature Measurements of Natural Surfaces using Infrared Radiometers," *Appl. Optics*, Vol. 7, No. 9, 1705-1710, 1968.
39. Federer, C. A., "Spatial Variation of Net Radiation Albedo and Surface Temperature of Forests," *J. Appl. Meteorology*, Vol. 7, No. 5, 789-795, 1968.
40. Fenn, R. W., *NATO Measurement Program on Optical Atmospheric Quantities in Europe (OPAQUE)*, Air Force Geophysics Laboratory, paper presented at Target Acquisition Symposium, U.S. Army Night Vision Laboratory, Ft. Belvoir, June 1976.
41. Hubbard, R., *H-O Target Acquisition Model Development and Evaluation*, Air Force Avionics Laboratory, paper presented at Target Acquisition Symposium, U.S. Army Night Vision Laboratory, Ft. Belvoir, June 1976.

REPORT DOCUMENTATION PAGE		READ INSTRUCTIONS BEFORE COMPLETING FORM
1. REPORT NUMBER <b>14</b> R-2016-PR	2. GOVT ACCESSION NO.	3. RECIPIENT'S CATALOG NUMBER <b>9</b>
4. TITLE (and Subtitle) <b>6</b> Atmospheric Visual and Infrared Transmission Deduced from Surface Weather Observations: Weather and Warplanes. VI.		5. TYPE OF REPORT & PERIOD COVERED Interim Rept.
7. AUTHOR(s) <b>10</b> R. E. Huschke		6. PERFORMING ORG. REPORT NUMBER
9. PERFORMING ORGANIZATION NAME AND ADDRESS The Rand Corporation 1700 Main Street Santa Monica, Ca. 90406		8. CONTRACT OR GRANT NUMBER(s) <b>15</b> F44620-73-C-0011
11. CONTROLLING OFFICE NAME AND ADDRESS FCRC Office (AF/RDXTR) Director of Planning, Programming & Analysis Hq USAF, Washington, D.C. 20330		12. REPORT DATE <b>11</b> Oct 1976
14. MONITORING AGENCY NAME & ADDRESS (if different from Controlling Office) <b>12</b> Hq P.		13. NUMBER OF PAGES 38
16. DISTRIBUTION STATEMENT (of this Report)  Approved for Public Release; Distribution Unlimited		15. SECURITY CLASS. (of this report)  UNCLASSIFIED
17. DISTRIBUTION STATEMENT (of the abstract entered in Block 20, if different from Report)  No restrictions		15a. DECLASSIFICATION/DOWNGRADING SCHEDULE
18. SUPPLEMENTARY NOTES		
19. KEY WORDS (Continue on reverse side if necessary and identify by block number) Weather Observations Atmospheric Attenuation Infrared Detectors Optical Detection		
20. ABSTRACT (Continue on reverse side if necessary and identify by block number)  see reverse side		

DD FORM 1473


EDITION OF 1 NOV 65 IS OBSOLETE

UNCLASSIFIED

SECURITY CLASSIFICATION OF THIS PAGE (When Data Entered)


296600

RECEIVED  
FEB 16 1977  
151



A quantitative method has been developed to evaluate meteorological data (surface weather observations) in terms of the performance of visual and infrared sensors so that relevant time and space variability in performance can be depicted. Approximate atmospheric transmission parameters for visible and infrared radiation are deduced from common weather observables (cloud data, temperature, humidity, etc.) as are vertical profiles of the parameters. Use of these algorithms with a set of target acquisition modeling equations (as given in Appendix A) can produce target detection probabilities for any location, season, and time scale for which historical-weather data are available. In turn, the detection probabilities can be employed in battle simulation models to examine how force effectiveness varies as a function of weather and climate.

(Auth.)



UNCLASSIFIED

SECURITY CLASSIFICATION OF THIS PAGE(When Data Entered)



**SUPPLEMENTARY**

**INFORMATION**

3-24-77

R-2016-PR ATMOSPHERIC VISUAL AND INFRARED TRANSMISSION REDUCED FROM  
SURFACE WEATHER OBSERVATIONS: WEATHER AND WARPLANES VI  
R. E. Huschke, October 1976 UNCLASSIFIED

The last sentence on p.30 of the report cited above, including the  
two displayed equations, should be replaced with the following:

AD-A036032

For elevated layers ( $i > 1$ ), sky-ground ratio  
is calculated from an inferred albedo,  $\rho_i$ , equivalent to the background  
reflectance calculated for the bottom of that layer. From the equa-  
tion for object brightness transmitted through a scattering layer, from  
the difference in downwelling illuminance between the upper and lower  
boundaries of the layer, and from the definitions of sky-ground ratio  
and reflectance, it can be shown that

$$\rho_i = e^{-B_{i-1}R_{i-1}} \left[ \rho_{i-1} e^{-B_{i-1}R_{i-1}} + (\hat{SG})_{i-1} \rho_{i-1} (1 - e^{-B_{i-1}R_{i-1}}) \right].$$

PUBLICATIONS  
DEPARTMENT

**Rand**  
SANTA MONICA, CA. 90406